IEICE Communications Express, Vol.13, No.7, 276–279

ComEX

LETTER

ISAR imaging for drone detection based on backprojection algorithm using millimeter-wave fast chirp modulation MIMO radar

Kenshi Ogawa[1, a)], **Dovchin Tsagaanbayar**[1], **and Ryohei Nakamura**[1]

Abstract In this paper, we propose an inverse synthetic aperture radar (ISAR) imaging method using a millimeter wave (mmW) fast chirp modulation (FCM) multi-input and multi-output (MIMO) radar for drone detection. To obtain high-resolution ISAR images, the backprojection algorithm is adopted for the ISAR processing. This algorithm is suitable for ISAR imaging of a moving drone with an irregular motion. The measurement experiments were conducted using flying drones (DJI Phantom 3, DJI Mavic Pro and DJI Mavic Mini) in indoor situations to examine the effectiveness of our proposal. The measurement results demonstrated that the proposed method could generate the high-resolution ISAR images enough to recognize the approximate size and shape of each drone.

Keywords: drone detection, millimeter-wave MIMO radar, fast chirp, radar imaging, inverse synthetic aperture radar, ultra-wideband
Classification: Sensing

1. Introduction

Drones have advanced rapidly and are widely used in various fields in recent years. However, along with their growing use, concerns have arisen about the possibility that drones can be abused for terrorism and crimes [1]. Therefore, antidrone systems must be able to detect and distinguish the threat drones. Radar is attracting significant attentions as an effective drone detection technology because they are not affected by weather conditions [2].

Several studies have been conducted recently on radar imaging for drone detection and classification [3, 4, 5]. Inverse synthetic aperture radar (ISAR), which is well-known technique for generating high-resolution radar images, has also been studied for drone detection. ISAR includes time domain and frequency domain image construction methods. In [3, 4], ISAR images of drones flying outside were constructed in the frequency domain. However, there are several challenges to construct ISAR images in the frequency domain: the complete motion compensation for complicated flight trajectory is generally difficult; large range migrations deteriorate image quality [6]. In particular, the challenge is accurate motion compensation for the irregular motion of a drone because the flight path of a drone is complicated by wind and maneuvers, making precise prediction difficult. The backprojection algorithm is a SAR digital reconstruction algorithm for synthetic aperture processing while compensating for the motion of a target in the time domain [7]. Compared to frequency domain algorithms, this algorithm can easily deal with the irregular motion in the motion compensation process and produce highly accurate images even when the range migration is large. To the best of our knowledge, no study on ISAR imaging of flying drone based on the backprojection algorithm has been reported. Therefore, the effectiveness of ISAR imaging based on this algorithm should be explored through a practical environment.

In this paper, we propose an ISAR imaging method based on backprojection algorithm using a millimeter wave (mmW) fast chirp modulation (FCM) multi-input and multi output (MIMO) radar for drone detection. The FCM MIMO radar achieves high range resolution by sweeping the frequency over an ultra-wide bandwidth and estimate the distance and direction of arrival (DOA) of a target simultaneously. The fast pulse repetition time also allows the radar to detect the detailed trajectory of a drone in a short period of time. High-resolution radar images can be generated by implementing the motion compensation based on the detailed trajectory information obtained by the radar. Indoor measurement experiments were conducted on three flying drones: DJI Phantom3, DJI Mavic Pro, and DJI Mavic Mini. In addition, the resulting trajectory and ISAR imagery are presented to investigate the effectiveness of our proposal for drone detection.

The rest of this paper is organized as follows. Section 2 is an explanation of ISAR imaging procedure using mmW FCM MIMO radar. Section 3 shows our measurement results and a discussion of the effectiveness of our proposal. Finally, we summarized this paper in Sect. 4.

2. ISAR imaging procedure

2.1 mmW FCM MIMO radar

Figure 1 shows a diagram of the mmW FCM MIMO radar. The FCM radar transmits and receives a sinusoid signal called chirp, whose frequency is modulated over an ultra-wide bandwidth with time. The chirp modulation time and observation time are called fast time and slow time, respectively. A received chirp is mixed with a transmitted chirp to measure the intermediate-frequency (IF) signal in each channel. The MIMO channel data are reconstructed into the MIMO virtual array which is single-input and multi-output channel data of a contiguous virtual array [8]. The range profiles showing distance from the radar to targets are estimated by performing a fast Fourier transform (range FFT)

[1] Dept. of Electronic and Information Engineering, National Defense Academy, Yokosuka-shi, Kanagawa 239-0811, Japan
[a)] ed22007@nda.ac.jp

DOI: 10.23919/comex.2024XBL0054
Received March 18, 2024
Accepted April 16, 2024
Publicized May 9, 2024
Copyedited July 1, 2024

on the IF signal obtained in each channel. The DOA can be estimated by performing a beamformer method over the indexes of the MIMO virtual array elements on all range bins of the range profiles [9]. Using the distance and DOA of a target measured by the radar, the rectangular coordinate $[x_l(t), y_l(t)]$ of a target at the t-th snapshot can be expressed as follows:

$$[x_l(t), y_l(t)] = [R(t)\sin(\theta), R(t)\cos(\theta)] \quad (1)$$

where, $R(t)$ and $\theta(t)$ are the slant range and DOA of the largest reflection point of a target at the t-th snapshot, respectively. Drone consisting multiple components have many scattering points. It follows that the largest reflection point of a drone changes depending on the positional relationship between the radar and the drone [5]. The coordinates $[x_l(t), y_l(t)]$ does not necessarily record a certain scattering point and therefore contains errors according to the size of drone. The random sample consensus (RANSAC) is a polynomial fitting method to estimate parameters of a model from the data that contains outliers, which exclude the outliers and find a suitable model [10]. To remove influence of the errors, the motion model $[x_m(t), y_m(t)]$ is estimated by modeling the coordinate $[x_l(t), y_l(t)]$ using the RANSAC method.

2.2 ISAR processing based on backprojection algorithm

The backprojection algorithm produces high-resolution ISAR images through range compression using range FFT, motion compensation, and azimuth compression using synthetic aperture processing. The motion compensation processing plays an important role in focusing the ISAR image. Figure 2 shows the ISAR processing flow based on backprojection algorithm. First, range compression using range FFT is performed for one channel data in the MIMO channel, calculating the range profile $s(u,t)$ of range bin u at each slow time t. Then, motion compensation and azimuth compression are processed simultaneously using the motion model in the previous section. ISAR image $Image(x_i, y_j)$ in the spatial domain (x_i, y_j) can be expressed as follows:

$$Image(x_i, y_j) = \int_t s[u_{ij}(t), t] e^{-j\frac{4\pi f_c}{c} R_e(x_i, y_j)} dt \quad (2)$$

$$R_e(x_i, y_j) = \sqrt{[x_i - x_m(t)]^2 + [y_j - y_m(t)]^2} \quad (3)$$

$$s[u_{ij}(t), t] \approx s(u, t) \quad (4)$$

where, f_c and c are the center frequency and speed of light, respectively. $R_e(x_i, y_j)$ is the Euclidean distance between a given reflector at any grid point (x_i, y_j) on spatial domain and the t-th spatial coordinate $[x_m(t), y_m(t)]$ in the motion model, which implies motion compensation in this algorithm. In Eq. (4), $s(u,t)$ is interpolated to reconstruct the $s[u_{ij}(t), t]$ so that the range bin $u_{ij}(t)$ correspond to the Euclidean distance in Eq. (3) at each slow time t.

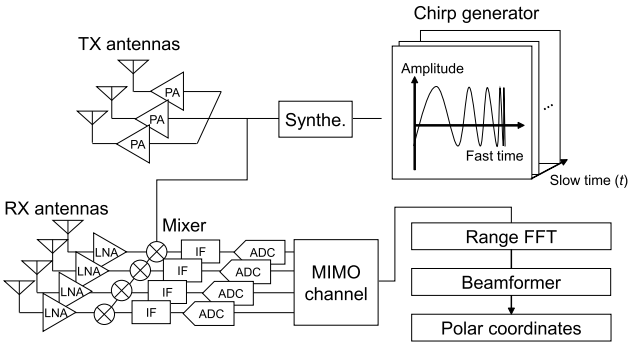

Fig. 1 mmW FCM MIMO radar.

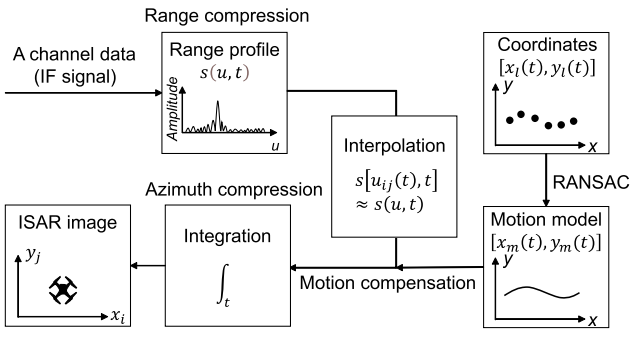

Fig. 2 ISAR processing flow.

3. Measurement experiments

3.1 Measurement setup

We tested three drones (DJI Phantom 3, DJI Mavic Pro, and DJI Mavic Mini) with different shapes and sizes as shown in Fig. 3 to generate ISAR images using a mmW FCM MIMO radar module. Table I shows the specifications of the radar and other parameters. The size of image cell for tracing the ISAR imagery was 0.8 m square (128 × 128 pixels). The number of range bin u was 1024 and was interpolated to range bin u_{ij}. Figure 4 shows the measurement environment. Drones were flown in manual mode with remote control indoor as shown in Fig. 4(a). Figure 5 shows the trajectory

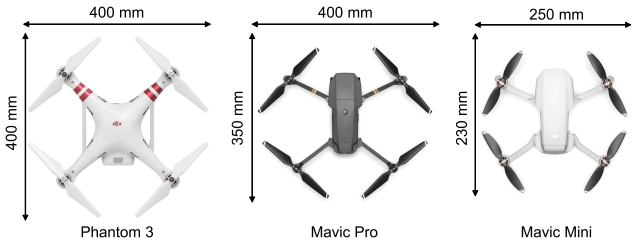

Fig. 3 Tested drones.

Table I Specifications of radar and parameter.

Array shape		Unfiorm linear array
Number of elements	Tx	3
	Rx	4
Antenna spacing	Tx	8 mm
	Rx	2 mm
Beamwidth	Azimuth	±35 deg
	Elevation	±4 deg
Center frequency f_c		78.72 GHz
Frequency bandwidth		3.44 GHz
Sweep time		57 μ s
Pulse repetition interval		0.97 ms
Image cell $x_i \times y_j$		128 × 128
Number of range bins u		1024
Number of range bins u_{ij}		16384

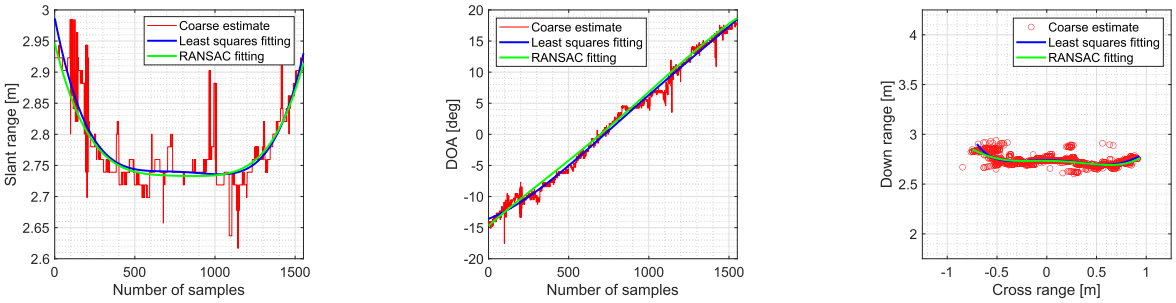

(a) Slant range (b) DOA (c) Rectangular coordinates

Fig. 6 Examples of polynomial fitting for a Phantom 3 trajectory.

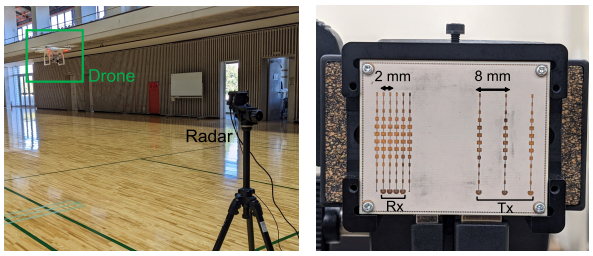

(a) Measurement scene (b) Radar module

Fig. 4 Measurement environment.

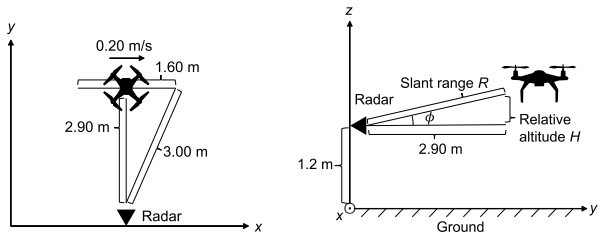

(a) x-y plane (b) y-z plane

Fig. 5 Reference trajectory.

of drones as a reference for the measurement. In the x-y plane, the squint angle of the radar was set to 0 degree, and drones were maneuvered to fly as straight as possible, as shown in Fig. 5(a). In the y-z plane, the elevation angle ϕ was set to 10 degrees for Phantom 3 and 5 degrees for Mavic Pro and Mavic Mini, and drones were controlled to maintain the same relative altitude H. The reason for difference of elevation angle ϕ depending on the drone is that the radar beam was aimed at a drone to cover its rear propellers. Since the drone was flown manually, its flight path was not strictly straight, and its speed and relative altitude was not constant, resulting in an irregular trajectory.

3.2 Measurement results and discussion

In order to verify how accurately the motion compensation based on the RANSAC method works in the ISAR process, the quality of ISAR imagery by the method is compared with that by the least squares method which is a basic method for data fitting. Figure 6 shows examples of polynomial fitting for the trajectory of Phantom 3. The red lines in Figs. 6(a) and (b) are the coarse estimate versus slow time (number of samples), which are obtained by measuring the largest reflection point of drone for each snapshot. There are sudden rises and drops that seem to differ from the actual flight path, thus, it is very likely that these estimates contain the outliers. The blue and green lines are the fitted curves modeled by the least squares method and the RANSAC method, respectively. Here, the coarse estimates are fitted to a fourth-order motion model using each of the fitting methods. The fitting results for the slant range are given in Fig. 6(a). We can see in this figure that the blue curve bent more rapidly than the green curve, as seen in the sample intervals from 0 to 250, and from 500 to 800. This is because the least squares method computes an approximate model for all measurement data contains outliers, decreasing the approximate likelihood. The fitting results for the DOA are shown in Fig. 6 (b). It can be seen from this figure that there is no significant difference between blue and green curves because the measurement data does not include the critical outliers. The results for the motion model can be expressed in rectangular coordinates with the horizontal axis as the cross range and the vertical axis as the down range, as shown in Fig. 6(c). The coordinates are transformed from the slant range (Fig. 6(a)) and DOA (Fig. 6(b)). We can see in Fig. 6(c) that the RANSAC method can produce the motion model which is more similar to reference trajectory than the least squares method. However, the actual flight path was not completely straight due to manual control, making it difficult to verify accuracy by comparing the motion model with the reference trajectory. Thus, the estimation accuracy is evaluated by the ISAR imaging quality which we discuss later.

Next, we turn now to show the generated ISAR images using each motion model. Figure 7 shows the ISAR images by the least squares method. The white solid lines in these figures are the overlays displaying the outline of each drone. The results show that these images provide rough and ambiguous outlines of the drones and that it is difficult to determine the exact size and shape of each drone. Moreover, there are ghost images at the coordinates where the drone does not exist. This is because the motion compensation error caused a shift of the focal point while constructing an ISAR image. We now turn our attention to the radar image of each of the drones by the RANSAC method, as shown in Fig. 8. For the Phantom 3, Fig. 8(a) shows that a footprint similar in shape to the overlay can be observed, and its approximate size can be estimated. Also, the signal strength from the rear is smaller than that from the front. This is both because the radar cross-section in front of the body is large due to the camera mounted in front of the body, and

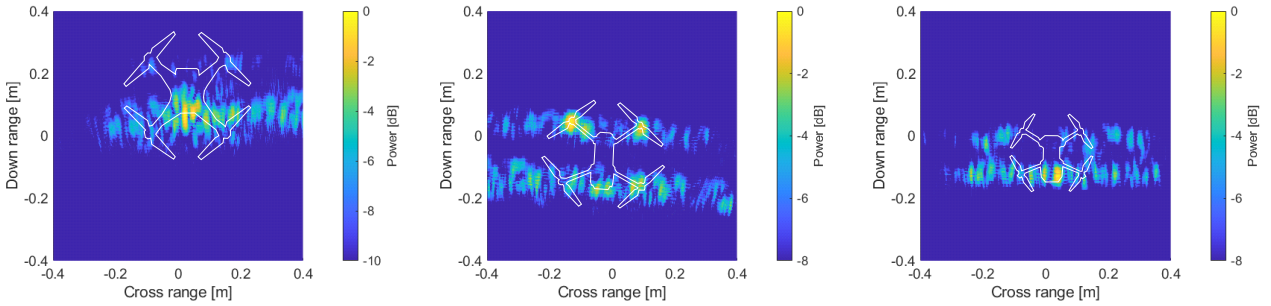

(a) Phantom 3 (b) Mavic Pro (c) Mavic Mini

Fig. 7 ISAR images by the least squares fitting.

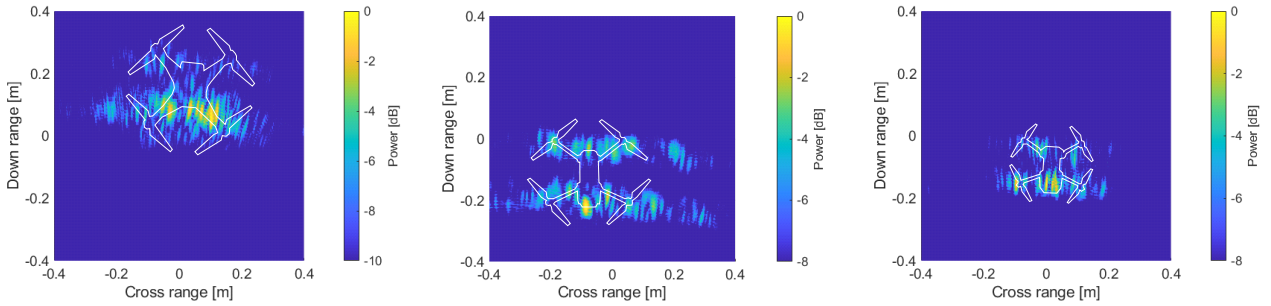

(a) Phantom 3 (b) Mavic Pro (c) Mavic Mini

Fig. 8 ISAR images by the RANSAC fitting.

because half of the rear arms is hidden by the body. For the Mavic pro, the drone shape and its four arms are clearly visible from Fig. 8(b). However, there are ghost images on the right side of the drone, attributed to the motion compensation errors. For the Mavic Mini, we can see a smaller foot print corresponding to its size than other drones, as shown in Fig. 8(c). These imaging results show that the well-focused image generation is achieved because the motion compensation is implemented accurately. Therefore, the accuracy of trajectory estimation by the RANSAC method is superior to that by the least squares method.

4. Conclusions

In this paper, we proposed an ISAR imaging method based on the backprojection algorithm using a mmW FCM MIMO radar for drone detection. In addition, to achieve accurate motion compensation in the ISAR processing, the RANSAC method was employed to model the trajectory of drone. To verify the effectiveness of the proposed method, measurement experiments were conducted on three types of drones in flight. The experimental results showed that the RANSAC method could accurately estimate the trajectory of drone. Furthermore, the ISAR could generate high-resolution radar imagery with a characteristic foot print relating to the size and shape of drone for drone detection.

Future research will focus on drone classification by applying deep learning to ISAR images.

Acknowledgments

This work was supported by JSPS KAKENHI Grant Number 21K04102.

References

[1] J.-P. Yaacoub, H. Noura, O. Salman, and A. Chehab, "Security analysis of drones systems: Attacks, limitations, and recommendations," *Internet of Things*, vol. 11, 100218, Sept. 2020. DOI: 10.1016/j.iot.2020.100218

[2] A. Coluccia, G. Parisi, and A. Fascista, "Detection and classification of multirotor drones in radar SensorNetworks: A review," *Sensors*, vol. 20, no. 15, 4172, July 2020. DOI: 10.3390/s20154172

[3] W.-K. Lee and K.-M. Song, "Enhanced ISAR imaging for surveillance of multiple drones in urban areas," Proc. 2018 International Conference on Radar, Brisbane, Australia, pp. 1–4, Aug. 2018. DOI: 10.1109/RADAR.2018.8557323

[4] C.J. Li and H. Ling, "Wide-angle, ultra-wideband ISAR imaging of vehicles and drones," *Sensors*, vol. 18, no. 10, 3311, Sept. 2018. DOI: 10.3390/s18103311

[5] C.J. Li and H. Ling, "An investigation on the radar signatures of small consumer drones," *IEEE Antennas Wireless Propag. Lett.*, vol. 16, pp. 649–652, July 2016. DOI: 10.1109/LAWP.2016.2594766

[6] K. Ouchi, *Principles of Synthetic Aperture Radar for Remote Sensing*, Tokyo Denki University Press, 2004 (in Japanese).

[7] M. Soumekh, *Synthetic Aperture Radar Signal Processing with MATLAB*, Wile-Interscience, 1999.

[8] J. Li and P. Stoica, "MIMO Radar Signal Processing," Wiley-IEEE Press, 2008. DOI: 10.1002/9780470391488

[9] S.U. Pillai, *Array Signal Processing*, Springer-Verlag New York, 2008.

[10] P.H.S. Torr and A. Zisserman, "MLESAC: A new robust estimator with application to estimating image geometry," *Computer Vision and Image Understanding*, vol. 78, no. 1, pp. 138–156, April 2000. DOI: 10.1006/cviu.1999.0832